An explicit robust optimization framework for multipurpose cascade reservoir operation considering inflow uncertainty

He, Shaokun; Wang, Yi Bo; Solomatine, Dimitri; Li, Xiao

DOI
10.1016/j.envsoft.2024.106301

Publication date
2024

Document Version
Final published version

Published in
Environmental Modelling and Software

Environmental Modelling and Software 185 (2025) 106301

Contents lists available at ScienceDirect

Environmental Modelling and Software

journal homepage: www.elsevier.com/locate/envsoft

An explicit robust optimization framework for multipurpose cascade reservoir operation considering inflow uncertainty

Shaokun He [a,c,d], YiBo Wang [b], Dimitri Solomatine [c,d,e], Xiao Li [a,f,*]

[a] State Key Laboratory of Water Resources Engineering and Management, Wuhan University, Wuhan, 430072, China
[b] Bureau of Hydrology, Changjiang Water Resources Commission, Wuhan, 430010, China
[c] IHE Delft Institute for Water Education, Delft, 2601DA, the Netherlands
[d] Water Resources Section, Delft University of Technology, Delft, 2600GA, the Netherlands
[e] Water Problems Institute of RAS, 119333, Gubkina 3, Moscow, Russia
[f] Hubei Provincial Key Lab of Water System Science for Sponge City Construction, Wuhan University, Wuhan, 430072, China

A R T I C L E I N F O

Keywords:
Multiobjective reservoir operation
Robust optimization
Inflow uncertainty
EMODPS
Robustness metric

A B S T R A C T

Long-term water resource management involving multipurpose coordination requires robust decision-making in water infrastructure cases to cope with various types of uncertainties. Traditional robust optimization methods generally do not explicitly propagate input or parametric uncertainties into estimates of the robustness of solutions, which limits their ability to address uncertainty comprehensively across solution spaces. In this study, we introduce an explicit robust decision-making framework that blends multiobjective search, probabilistic analysis of robustness, and diagnostic verification tools to identify robust optimal solutions to external uncertainty. The proposed framework is illustrated on four diverse robustness formulations, which capture a wide variety of stakeholder attitudes from highly risk-averse to risk-neutral, for the primary operating objectives (hydropower production, water diversion, and hydrological alteration degree) in China's Hanjiang cascade reservoir system. By analyzing the Pareto front propagated from inflow uncertainty, it is found that optimal robust policies with a significantly higher degree of hydrological alteration are preferred in most formulations to achieve relatively lower joint uncertainty of hydropower and water diversion. These policies also yield sufficiently stable model performance in the case of an out-of-sample streamflow set during diagnostic verification. Furthermore, a comparative analysis of four different formulations suggests that a composite normalized robustness indicator (*NRI*) developed in this study to integrate various robustness metrics can achieve an effective balance for all considered objectives. These findings highlight the benefits of explicit robust optimization for managing hydrological uncertainties in multipurpose cascade reservoirs.

1. Introduction

Persistent hydrometeorological variability at both intra-annual and interannual scales poses a significant challenge to water resource management. This challenge is particularly acute in developing countries, which rely heavily on water-related industries for socioeconomic development but often have inadequate infrastructural capacities to adapt to variable hydrological conditions (Jaiswal et al., 2021). The involvement of multiparty water interests is also expected to exacerbate the challenge, as it is often difficult to reach consensus on reallocating water resources across multiple sectors. To mitigate or even overcome the negative impacts of water conflicts associated with regional hydrological changes, it is urgent to explore more innovative water management policies (McPhail et al., 2021; Yu et al., 2023).

In this context, robust multipurpose operation of reservoirs has received attention in the past decade since multiple reservoirs have been built in many large river basins to regulate flows. Robust optimization operations can reap tremendous profits without additional engineering investments (He et al., 2022b). It strives to develop robust operating policies to achieve multifaceted water resource objectives while ensuring minimal discrepancies between the expected and actual consequences in plausible future states. Giuliani and Castelletti (2016) designed specific types of robust policies based on Gaussian radial basis function (RBF) approximators for Lake Como in Italy. Wang et al. (2023) improved the robustness of dam infrastructure by updating the operating diagram to better accommodate deep uncertainties arising from

* Corresponding author. State Key Laboratory of Water Resources Engineering and Management, Wuhan University, Wuhan, 430072, China.
E-mail address: xiao.li8@mcgill.ca (X. Li).

https://doi.org/10.1016/j.envsoft.2024.106301
Received 14 June 2024; Received in revised form 5 December 2024; Accepted 9 December 2024
Available online 10 December 2024

climate change and the electricity market. These findings indicated that robust operating policies could help mitigate certain changes in the hydrological cycle, especially when compared to conventional policies derived from historical observations that yield poor performance in possible future scenarios. However, the primary goals are often associated with developing state-of-the-art modeling approaches or policy styles, and the effects of the problem formulation chosen on the outcomes of alternative policies and subsequent assessments of optimal solutions are rarely considered (Wu et al., 2023). McPhail et al. (2018) found that some robustness problem formulations would miss all optimal decision-relevant solutions. This phenomenon has inspired reservoir managers to investigate various problem formulations in the participatory planning process to identify the most robust and optimal policies considering diverse stakeholder perceptions.

The common types of robustness formulations include expectation, regret-based, higher-order moment (e.g., variance and skewness), and satisficing formulations (McPhail et al., 2018). These formulations capture a gradient of stakeholder risk preferences across scenarios from highly risk-averse (e.g., min-max regret) to risk-neutral (e.g., expected value). For a specific case, the problem framework stakeholders establish had better consider all relevant formulations that can effectively reflect their risk attitudes (Kwakkel et al., 2016; Marquez Calvo, 2020). It is also essential to reevaluate the performance of the resulting policies associated with each formulation in other rival formulations to mitigate unintended systematic biases (Quinn et al., 2017). Building on this principle, Bonham et al. (2024) conducted an experiment in the Colorado River Basin using a comprehensive robustness analysis framework encompassing expectation, regret-based and satisficing robustness metrics to evaluate the potential performance of Lake Mead shortage policies over future scenarios. Ultimately, they identified a policy with balanced performance across all metrics. However, this approach will inevitably increase computational demands, particularly as the number of robustness metrics to be evaluated grows. Recent studies in water fields have begun to explore composite robustness metrics to tackle these challenges (Sunkara et al., 2023; Zhang et al., 2024b). These metrics aim to simultaneously account for multiple robustness aspects within a single evaluative framework, thereby reducing redundant calculations and improving consistency across evaluations. The development of such a comprehensive robustness metric is of paramount importance, not only to mitigate computational burdens but also to enhance the applicability of robustness analyses in complex, scenario-rich decision-making environments. Under this background, we first used a composite normalized robustness index (*NRI*) we developed as one of the robustness optimization objectives, which can theoretically integrate all robustness metrics to evaluate the effectiveness of our robust framework.

Moreover, an effective optimization method is deemed critical to accommodate such a constructive robustness framework. Given the high-dimensional and stochastic nature of robust control problems, a viable method is favored if it can mitigate the curse of dimensionality from reservoir number and exogenous uncertainty. Quinn et al. (2019) demonstrated the effectiveness of Evolutionary Multiobjective Direct Policy Search (EMODPS) combined with multiobjective evolutionary algorithms (MOEAs) in addressing hydrological variability for robust management of food-energy-water conflicts. Recent advancements in our computational power to solve multiobjective optimization problems (He et al., 2022a) have significantly expanded the applicability of a large number of EMODPS implementations, enabling its broader integration within the robustness framework.

In this study, we adopt a variant of robust optimization and probabilistic analysis of robustness (ROPAR) (Marquez and Solomatine, 2019) for our EMODPS-based robustness optimization. Unlike other common implicit algorithms (e.g., implicit robust optimization (Quinn et al., 2017) or smoothing optimization (Kapelan et al., 2005)) that embed the impact of uncertainty into a single Pareto front, ROPAR describes the uncertainty of outcomes in terms of an explicit visualization of all Pareto front distributions. ROPAR allows for a fuller exploration of the Pareto solution space and can approximate objective robustness through solution clouds (Marquez and Solomatine, 2019). Zhang et al. (2024b) applied ROPAR to a classical two-objective water resource allocation system that achieved a robust trade-off between water deficit and ecological needs. However, in cases with more water interests involved, it remains doubtful whether an extended ROPAR algorithm can have value for decision-makers. Overall, we develop an explicit decision-making framework that considers diverse robustness formulations to identify robust policies by tackling the following questions: (1) How effective is our explicit multi-dimensional optimization framework in finding robust policies, particularly in the *NRI*-dominated robustness formulation? (2) How does our presented robustness method differ from other representative robust optimization methods?

To answer these questions, we choose a cascade reservoir system in the Hanjiang River basin in China as our case study. The remainder of this article is structured as follows. In section 2, a brief description of the study basin is given, and the associated model profile is introduced. The procedures of our robust decision-making framework are elaborated in section 3. In section 4, an analysis of how ROPAR policies designed with different formulations perform in plausible future states is provided. Finally, the main conclusions are presented in section 5, along with a discussion of potential prospects.

2. Case study

2.1. Hanjiang River basin

As the largest tributary of the Yangtze River, the Hanjiang River encompasses a catchment area of 159,000 km^2, with a river length of 1577 km. It serves as a vital socioeconomic resource for this developing nation. A series of water conservancy facilities, such as the middle route of the south-to-north water transfer (MSWT) project and some reservoirs, have been built in the river system to facilitate water resource development. Specifically, an official water diversion diagram in the basin was customized by the Ministry of Water Resources of China to alleviate water shortages in the North China Plain (MWR, 2016). As shown in Fig. 1, the diagram is divided into five different zones. Each zone has a corresponding preset value for water diversion discharge, namely, 420 m^3/s for Zone I, 350 m^3/s for Zone II, 300 m^3/s for Zone III, 260 m^3/s for Zone IV, and 135 m^3/s for Zone V. Note that this portion of diversion discharge is conveyed through some special pipelines instead of flowing into the turbines at Danjiangkou Reservoir (Fig. 2(b)). Consequently, diversion of water through the MSWT project and maximization of hydropower benefits in the river system are two competing objectives.

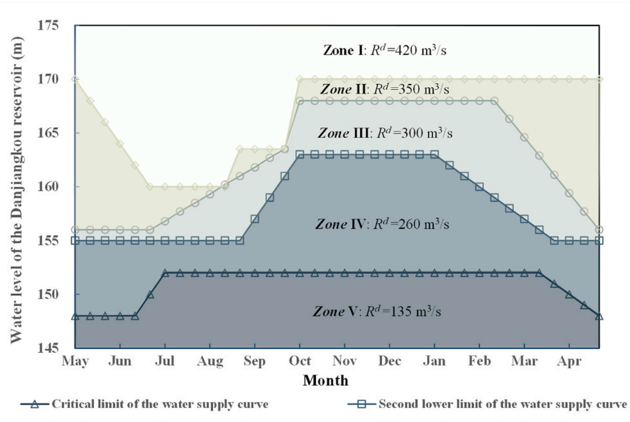

Fig. 1. Water diversion diagram of the Danjiangkou Reservoir for the Middle Route of the South-to-North Water Transfer (MSWT) project.

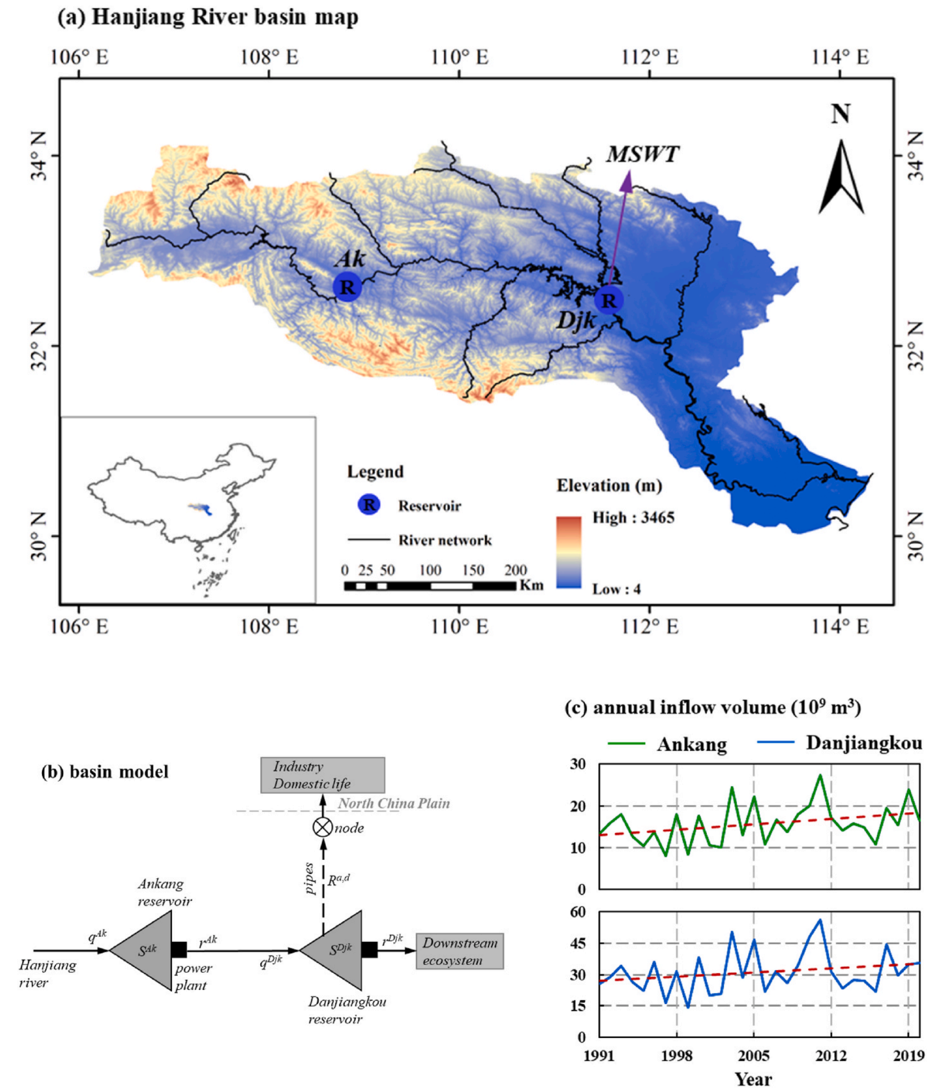

Fig. 2. (a) Map of the Hanjiang River basin; (b) Schematization of the main components of the basin model; (c) Annual inflow volumes of the Ankang (*Ak*) and Danjiangkou (*Djk*) Reservoirs during 1991–2020.

Apart from these two operating objectives, river system managers are concerned with the impact of flow regime alteration in recent years, as anthropogenic disturbances have been found to negatively affect riverine ecosystems (He et al., 2023). A substantial transregional water diversion can considerably diminish downstream water volume, resulting in a poor performance on the Indicators of Hydrological Alteration (IHA) that reflects overall ecological conditions (Zhang et al., 2024a). In this study, we investigate whether improved multireservoir operation in the Hanjiang River basin can effectively reconcile the multisectoral demands among transregional water diversion, hydropower production, and environmental conservation.

2.2. Model profile

The Ankang and Danjiangkou Reservoirs are connected in series along the main stem (Fig. 2(a)). The annual runoff varies greatly, with coefficient of variation (*CV*) values of 0.29 and 0.32 (Fig. 2(c)), respectively. To utilize these unevenly distributed water resources, the cascade reservoirs have a total storage capacity of 36.38 billion m^3 and a total power capacity of 1750 MW. The upstream Ankang (*Ak*) Reservoir primarily serves for hydropower generation. The downstream Danjiangkou (*Djk*) Reservoir involves more industry and domestic uses. The combined reservoir system is designed to resist floods during the flood season, alleviate water supply deficits during the dry season, and improve hydropower production as well as the ecological environment between seasons. More details of these reservoirs are shown in Table 1.

In this model, flows through the Hanjiang River basin, mainly considering flows through the reservoirs, river channel, and canal of the MSWT project, are simulated. The volume of storage s_t^i of these reser-

Table 1
Characteristic parameters of the Ankang and Danjiangkou Reservoirs.

Reservoir characteristics	Unit	Ankang	Danjiangkou
Total storage capacity	billion m^3	3.34	33.04
Flood control capacity in summer/autumn	billion m^3	0.36	14.10/11.10
Crest elevation	m	338.0	176.6
Normal water level	m	330.0	170.0
Flood-limited water level in summer/autumn	m	325.0	160.0/163.5
Dead water level	m	305.0	150.0
Maximum power capability	MW	850	900
Primary function	–	*HG, FC*	*FC, WD, HG, & ER* [a]

[a] *FC*, *WD*, *HG* and *ER* represent flood control, water diversion, hydropower generation and ecological regulation, respectively.

voirs at time $t+1$ is estimated by the physical mass balance equation:

$$s_{t+1}^{Ak} = s_t^{Ak} + \left(q_t^{Ak} - r_t^{Ak}\right) \cdot \Delta t - ES_t^{Ak} \tag{1}$$

$$s_{t+1}^{Djk} = s_t^{Djk} + \left(q_t^{Djk} - R_t^{a,d} - r_t^{Djk}\right) \cdot \Delta t - ES_t^{Djk} \tag{2}$$

where q_t^i and r_t^i are the inflow and actual release of the ith reservoir during the time interval $[t, t+1)$, respectively, $R_t^{a,d}$ and ES_t^i are the actual diversion discharge and water loss (e.g., evaporation and infiltration) of the ith reservoir during this time interval, respectively, Δt is the time step. Three operating objectives are summarized in Table 2: (1) hydropower output at each time step is calculated with the output equation $\eta_t^i = min\left(9.81\gamma^i Q_t^i H_t^i, P_{max}^i\right)$, where the function $min(\cdot)$ refers to taking the minimum value, γ^i is the power coefficient, Q_t^i is the power release, H_t^i is the hydraulic head, and P_{max}^i is the maximum allowable output, (2) water diversion volume is aggregated by actual diversion flow $R_t^{a,d}$, and (3) the degree of hydrological alteration, $D = \sqrt{\frac{1}{H}\sum D_h^2}$ (further details in Section 3.1.1 and Supplementary Text S2), arising from reservoir operations is determined from actual Danjiangkou Reservoir release sequences r_i^{Djk}.

Since it is unrealistic and unsafe to assume that future streamflow will not deviate from historical observations (Giuliani et al., 2016), we perform a systematic simulation over $N = 300$ ensemble members and $T = 30$ years (i.e., 300 unique 30-year streamflow sequences) for synthetically generated hydrological series. Here, we assume hydrologic stationarity in the synthetic flows since the Mann-Kendall tendency of historical series is insignificant at a significance level of $p < 0.05$ (Fig. 2 (c)). First, we simultaneously generate monthly flows using a Cholesky decomposition of resampled historical flows, maintaining spatial and autocorrelation as per Kirsch et al. (2013). Second, we disaggregate monthly flows into 10-day flows using Nowak et al. (2010)'s nearest-neighbor approach, which preserves synthetic monthly totals based on the probabilistic selection of the k nearest neighbors in the historical monthly record and proportional scaling of historical 10-day flows at each site. The validation of these synthetic flows is provided in the Supplementary Material.

3. Methodology

In this section, the EMODPS method is used to identify robust operating policies across four robustness problem formulations. As illustrated in Fig. 3, the main modules include: (1) problem formulation focusing on the robustness of system objectives, particularly the *NRI*-dominated formulation, (2) parameterization of reservoir operating policies, (3) explicit robust optimization of these policies, and (4) diagnostic verification of the optimized policies. Each module is detailed in the subsequent subsections.

3.1. Problem formulations with different robustness objectives

Different robustness formulations reflecting different decision-makers' attitudes may lead to different or even contradictory decisions. Referring to Quinn et al. (2017), we develop four candidate formulations representing a range of stakeholder risk preferences: (1) expected value (*EV*), (2) second-worst (*SW*), (3) expected value & standard deviation of water diversion ($EV\&SD_{WD}$), and (4) expected value & normalized robustness indicator of water diversion ($EV\&NRI_{WD}$). These formulations can represent a broad spectrum of attitudes, from highly risk-averse to risk-neutral.

In each formulation, the simulation of operating policies is performed over N ensemble members and T years of synthetic flows, with each T-year simulation starting on May 1st, the first day of the monsoon season, and ending on April 30th. The general mathematical formula for assessing the performance of the dth objective across the nth member of T-year simulations ($J_d(n)$) is shown below.

$$J_d(n) = \Psi^d_{Y\in(1,\ldots T)}\left[\Phi^d_{t\in(1,\ldots,36)}\left[g_d(t, Y, n)\right]\right], \quad n \in (1, \ldots, N) \tag{3}$$

where $g_d(t, Y, n)$ is the dth objective of the nth ensemble member in the tth period of the Yth year, Φ^d is an operator for the aggregation of $g_d(t, Y, n)$ within an annual operating horizon ($t \in 1,\ldots,36$), e.g., the sum (Σ), and Ψ^d is a statistic used to filter the noise over ensemble members, e.g., the mean or the 90th percentile. The optimal operating policy p_θ^* satisfies the high-dimensional objective optimization condition, which is described below.

$$p_\theta^* = arcmax\, \boldsymbol{J}_{p_\theta} \tag{4}$$

where θ is a vector of decision variables describing the operating policy set p_θ (defined in section 3.2) and $\boldsymbol{J}_{p_\theta}$ is the objective vector of $\left[J_{Hydro}(p_\theta), J_{WD}(p_\theta), -J_{Eco\_Alt}(p_\theta)\right]^{\mathrm{T}}$, where J_{Eco_Alt} with a negative sign indicates that a smaller value is preferred (see details in Supplementary Text S2). More descriptions for each optimization objective under each formulation are provided in sub-sections 3.1.1–3.1.4.

3.1.1. Expected value (EV) formulation

The *EV* formulation, known as Laplace's principle of insufficient reason (Laplace and Simon, 1951), assumes a risk-neutral operator who is concerned with the average performance of operating objectives across plausible future states. In the *EV*, the first objective, J_{Hydro}^{EV}, involves maximizing annual average hydropower production, which supports the goal of the Central China State Grid to generate cleaner hydropower to substitute for nonrenewable fossil fuels. The *EV* optimization of hydropower is performed across a 300-member ensemble over 30 years of simulation ($\Phi^{Hydro} = \sum_{t=1}^{36}$ and $\Psi^{Hydro} = E_T$). A simulation period of 30 years is set to ensure that enough hydrological regimes are considered to generate optimal policies that can be generalized to unknown hydrological conditions. An ensemble of 300 simulations over 30 years can provide adequate flow samples for the reasonable performance of optimal policies during a potential long-term planning period (Labadie, 2004). For cascade reservoirs, we maximize hydropower generation rather than revenue because the local electricity market is regulated by the government and energy is sold at a fixed price of 0.21 RMB/kWh. The maximization of both is essentially the same once the price is fixed.

The second objective, J_{WD}^{EV}, involves maximizing the annual average water diversion volume. As with hydropower, the operator is set to $\Phi^{WD} = \sum_{t=1}^{36}$, and $\Psi^{WD} = E_T$ over each ensemble member of the synthetically generated streamflow series. It assumes that the operators expect the MSWT project to play a long-term role in relieving water shortages in the North China Plain (Long et al., 2020). The market price of water diversion from MSWT is 0.13 RMB/m^3.

The final objective of this formulation, $J_{Eco\_Alt}^{EV}$, is to minimize the degree of hydrological alteration. Unlike the first two cumulative optimization objectives, this objective requires the altered streamflow condition (reservoir outflow) to be as consistent as possible with the natural condition (natural inflow). From a quantitative perspective, the IHA index that describes flow regimes based on magnitude, duration time,

Table 2
Three operating objectives of the cascade-reservoir system.

Objective	Unit	Calculating equation	Key variable [a]
Hydropower generation	kWh	$\sum min\left(9.81\gamma^i Q_t^i H_t^i, P_{max}^i\right)$	Q_t^i
Water diversion	m^3	$\sum R_t^{a,d}$	$R_t^{a,d}$
Hydrologic alteration degree	–	$\sqrt{\frac{1}{H}\sum D_h^2}$	r_t^{Djk}

[a] "Key variable" refers to the critical variable that directly determines the corresponding operating objective performance in the cascade-reservoir system.

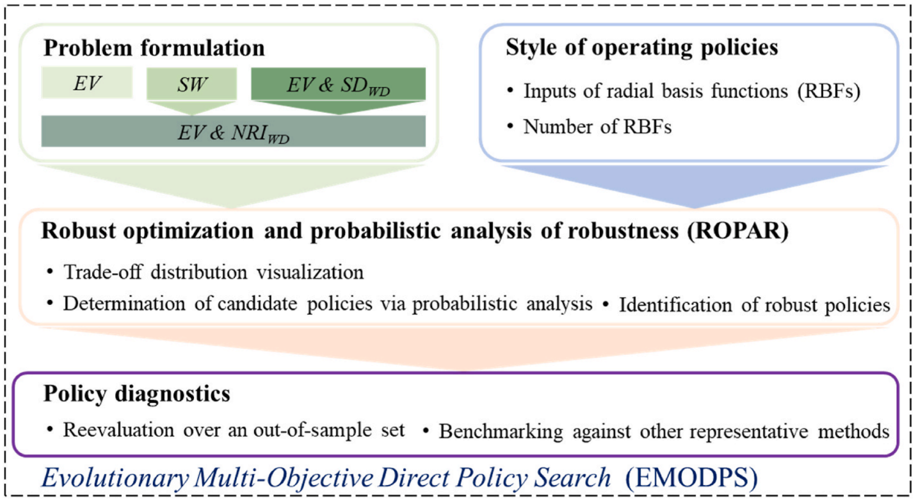

Fig. 3. Main modules for identifying robust operating policies via the EMODPS method.

the timing of extreme flows, and frequency, can be used for this objective (Mohanty and Tare, 2022). The IHA parameters are listed in Table S1, and $J^{EV}_{Eco\_Alt}$ is calculated with Eq. (S2). The corresponding operator Φ^{Eco_Alt} is related to annual outflow sequences ($\{\cdot\}$), and the statistic Ψ^{Eco_Alt} is set to a time series over T consecutive years ($\{\cdot\}$).

3.1.2. Second-worst (SW) formulation

The *SW* formulation targets the tail performance of the system. The concept was first proposed by Savage (1951), who assumed a risk-averse attitude that guarantees a certain security level even in case of extremely adverse scenarios. It should be noted that unlike a traditional worst-case (*WC*) formulation consisting of a 9000-member ensemble and 1-year simulations, we keep its synthetic hydrology same as in *EV*. The motivations are threefold: (1) comparisons of these formulations can focus on the specific optimization policies themselves if the same synthetic hydrological series are used; (2) The *SW* across 30 years could be more stable than worst-case (*WC*) in the same sampling size, where the latter has a higher sampling variance and may be unbounded. Prior studies re-evaluated the policies derived from *SW* and *WC*, respectively, on an out-of-sample streamflow set, and the results indicated that policies from *WC* cannot be effectively generalized (Giuliani et al., 2018; Quinn et al., 2017); and (3) aggregating objectives over the 30-year simulation is more appropriate for long-term reservoir management, especially for hydrological streamflow alteration that is of little significance in 1-year simulations.

In the *SW* formulation, we calculate annual hydropower generation and water diversion volume for each year within each ensemble member, i.e., $\Phi = \sum_{t=1}^{36}$. We then maximize the corresponding objective values in the *SW* case over 30 years (i.e., $\Psi = \text{quantile}_{T,sw}\{\Phi\}$), which is equivalent to maximizing the values over a 29-year return period. $J^{SW}_{Eco\_Alt}$ is the same as that in *EV* because hydrological alteration is a long-term ongoing process.

3.1.3. Expected value and standard deviation of water diversion ($EV\&SD_{WD}$) formulation

The $EV\&SD_{WD}$ formulation offers a compromise between the risk-neutral *EV* and risk-averse *SW* formulations, with an additional perspective on the interannual variability of water diversion volume across multiple scenarios. It is designed to meet the national strategic requirement for the region, ensuring a stable water supply capability (Long et al., 2020). In the traditional optimization literature, it has long been acknowledged that there are often contradictory interactions between zero-order moment (mean) and high-order moments (e.g., variance and skewness) of stochastic performance measures (Pinto et al., 2019). Therefore, decision-makers are sometimes willing to sacrifice exceptionally good years of water diversion if long-term management policies can mitigate exposure to drought-induced diversion losses. In water-related fields, these concerns have been eliminated by including measures of variability other than expectation, either as additional objective functions related to the robustness of multiobjective optimization (Roach et al., 2016), as constraints (Deb and Gupta, 2006), or through comparisons of the cumulative distribution functions of alternatives (Marquez Calvo, 2020). In this formulation, we take the first method and explicitly quantify the relationship between maximizing the expected value of the annual water diversion volume and minimizing its standard deviation by adding an extra objective to the *EV* formulation: $J^{EV\&SD_{WD}}_{SD_{WD}}$ ($\Phi = \sum_{t=1}^{36}$ and $\Psi = std_T$). All other objectives and constraints are the same as those in the *EV* formulation.

3.1.4. Expected value and normalized robustness indicator of water diversion ($EV\&NRI_{WD}$) formulation

The final formulation we propose here is to develop a composite *NRI*, which is designed to simultaneously optimize the *SW* and *SD* metrics for water diversion. This formulation replaces the optimization objective $J^{EV\&SD_{WD}}_{SD_{WD}}$ in $EV\&SD_{WD}$ with $J^{EV\&NRI_{WD}}_{NRI_{WD}}$, while keeping all other objectives identical. For the *SW* and *SD* metrics of water diversion, there are two options for obtaining *NRI*: linear weighting or by measuring the Euclidean distance from the origin in the space of the two metrics. We use the first easy-to-calculate approach to aggregate the *NRI*, as shown in Eq. (5).

$$NRI_{WD}(x) = (NormSW_{WD}(x) + NormSD_{WD}(x))\,/\,2 \tag{5}$$

where SW_{WD} and SD_{WD} are assumed to be equally important. The *NRI* varies from 0 to 1; the larger the value is, the more robust the corresponding solution x is. The normalization of the two metrics ($NormSW_{WD}$ and $NormSD_{WD}$) is performed as follows.

$$NormSW_{WD}(x) = \frac{SW_{WD}(x) - min(SW_{WD})}{max(SW_{WD}) - min(SW_{WD})} \tag{6}$$

$$NormSD_{WD}(x) = \frac{max(SD_{WD}) - SD_{WD}(x)}{max(SD_{WD}) - min(SD_{WD})} \tag{7}$$

where $max(SW_{WD})$ and $min(SW_{WD})$ are the preset maximum and minimum thresholds of *SW* water division, respectively, $max(SD_{WD})$ and $min(SD_{WD})$ are the maximum and minimum possible standard deviations of water division, respectively. Another general type of satisficing robustness formulation is not considered here because it refers to decision-maker's tendency to seek outcomes with acceptable performance relative to a threshold. However, the adaptation of our reservoir regulation has no cost, and consequently, the decision-makers will naturally adapt to achieve optimal performance.

A summary of these objective calculations for each formulation is given in Table 3.

3.2. RBF-based reservoir operating policies

To best meet all the objectives defined in sub-sections 3.1.1-3.1.4, we need to specify a form of operating policy that describes release decision as a function of time-varying inputs. We determine RBFs because of their reported scalability with respect to the state-decision space and past observed success in generating policies that can be effectively validated with out-of-sample sets (Giuliani et al., 2016; Quinn et al., 2019). The RBF-based policy representation is expressed in Eq. (8), where u_t^i is the policy-designated release for the ith reservoir at time t (normalized to [0, 1]), $(X_t^i)_m$ is the value of the mth of M time-varying inputs at time t for the ith reservoir (normalized to [0, 1]), and w_k^i, $c_{k,m}^i$, and $b_{k,m}^i$ are the weights, centers, and radii of K RBFs associated with the ith reservoir, respectively.

$$u_t^i = \sum_{k=1}^{K} w_k^i \exp\left[-\sum_{m=1}^{M} \frac{\left((X_t^i)_m - c_{k,m}^i \right)^2}{b_{k,m}^i} \right] \tag{8}$$

where $w_k^i \in [0, 1]$ with $\sum_k^K w_k^i = 1\ \forall i$, $c_{k,m}^i \in [-1,1]$, and $b_{k,m} \in (0,1]$. We model reservoir releases using 3 inputs: reservoir storage, reservoir inflow and time within a water year. The number of RBFs, K, is determined by an exhaustive search process, i.e., increasing K until the indicator (e.g., hypervolume) of the Pareto front of traditional deterministic optimization does not significantly change (see Text S3 for more details).

3.3. The multiobjective ROPAR algorithm

The ROPAR algorithm, first proposed by Marquez and Solomatine (2019) for two-objective robust optimization, enables an explicit visualization of uncertainty propagation from model inputs to the outputs of optimal solutions. It can discover robust solution clouds through probabilistic analysis. Here, it is adopted and extended to solve our robust three-objective optimization after validating against a benchmark

Table 3
Summary of the four formulations considered in this study.

Formulation	Original reference	Objective	Scenario	Φ	Ψ
EV	*Laplace and Simon* (1951)	J_{Hydro}^{EV}	All	$\sum_{t=1}^{36}$	E_T
		J_{WD}^{EV}	All	$\sum_{t=1}^{36}$	E_T
		$J_{Eco\_Alt}^{EV}$	All	$\{\cdot\}$	$\{\cdot\}$
SW	*Savage* (1951)	J_{Hydro}^{SW}	Second worst	$\sum_{t=1}^{36}$	$\text{Quantile}_{T,SW}$
		J_{WD}^{SW}	Second worst	$\sum_{t=1}^{36}$	$\text{Quantile}_{T,SW}$
		$J_{Eco\_Alt}^{SW}$	All	$\{\cdot\}$	$\{\cdot\}$
EV&SD$_{WD}$	Quinn et al. (2017)	$J_{Hydro}^{EV\&SD_{WD}}$	All	$\sum_{t=1}^{36}$	E_T
		$J_{WD}^{EV\&SD_{WD}}$	All	$\sum_{t=1}^{36}$	E_T
		$J_{Eco\_Alt}^{EV\&SD_{WD}}$	All	$\{\cdot\}$	$\{\cdot\}$
		$J_{SD_{WD}}^{EV\&SD_{WD}}$	All	$\sum_{t=1}^{36}$	std_T
EV&NRI$_{WD}$	*Marquez Calvo, 2020*	$J_{Hydro}^{EV\&NRI_{WD}}$	All	$\sum_{t=1}^{36}$	E_T
		$J_{WD}^{EV\&NRI_{WD}}$	All	$\sum_{t=1}^{36}$	E_T
		$J_{Eco\_Alt}^{EV\&NRI_{WD}}$	All	$\{\cdot\}$	$\{\cdot\}$
		$J_{NRI_{WD}}^{EV\&NRI_{WD}}$	All	$\sum_{t=1}^{36}$	*NRI*

function (see Text S4). The procedure of the ROPAR algorithm is shown in Fig. 4, and the main steps are summarized below.

Step 1: For uncertain inputs ε (specifically, reservoir inflow in this study), they are randomly generated N times to form an ensemble of N members. For each deterministic member ε_n ($n = 1, 2, ..., N$), the corresponding Pareto-optimal subset F_n is determined through individual multiobjective optimization, where F_n denotes the vector of all objective functions $\left(f_{1,n}, ..., f_{r,n}\right)$.
Step 2: Initially, select an objective function f_i ($i \in [1, 2, ...r]$); it is designated as the nonpivotal objective function, while the remaining objectives (or parts thereof) are considered pivotal. Choose an arbitrary level L for the nonpivotal function, and then select a solution closest to this level from each Pareto set F_n to construct the candidate solution set Λ.
Step 3: Build an empirical distribution based on the values of the pivotal functions from the members of set Λ. The empirical distribution can be used to approximate the joint probability density function (pdf) characterizing the uncertainty of the pivotal functions at the chosen level L. A narrower empirical distribution indicates less sensitivity of the pivotal objectives to stochastic inputs, thereby signifying greater robustness.
Step 4: Repeat steps 2–3 with various levels L to replace the candidate set Λ, until finding the optimal level of the nonpivotal function, characterized by the minimum variance of the empirical distribution, which mathematically quantifies the narrowness described in Step 3.
Step 5: Create the final set Λ' once the final level L is determined. Λ' should contain one optimal solution from every F_n with the final level L.
Step 6 (optional): Select another objective function to be nonpivotal and (parts of) others to be pivotal. Repeat steps 2–5 to expand Λ' until all nonpivotal objectives are traversed.
Step 7: Finally, the robust solution is determined from Λ' by measuring certain aggregation criteria of pivotal functions over the N-member ensemble, such as the aggregated economic benefit of hydropower generation and water diversion in this study.

The implementation of ROPAR employs MOEAs as its core optimizer in full multiobjective optimization. Among these MOEAs, the non-dominated sorting genetic algorithm version III (NSGA-III) (Deb and Jain, 2014) has gained recent prominence for its exceptional search capabilities, especially in high-dimensional optimization space (Dariane et al., 2021). It exploits global probabilistic operators for mating, mutation, and selection processes, and incorporates the concept of reference points to preserve solution diversity. Specifically, NSGA-III is applied to optimize policy parameters, setting the hyperparameter values to 200 for population size and 1000 for the number of generations.

3.4. Diagnostic verification of optimized policies

The final module of EMODPS focuses on the diagnostic validation of optimized policies from section 3.3. It involves two main aspects: (1) re-evaluating these control policies against an out-of-sample set of plausible streamflow ensembles, and (2) contrasting them with those generated using common robust techniques to highlight their differences. In addressing the first case, we generated an expanded ensemble of stochastic streamflow, comprising 3000 members of 30-year synthetic streamflow, which is ten times the number of ensemble members used during optimization. ROPAR policies are considered truly robust if they achieve optimal results in re-evaluation akin to those in optimization, i.e., achieving the optimal pivotal objective performance and maintaining a narrow joint pdf.

We also assess the performance of robust optimal policies from each

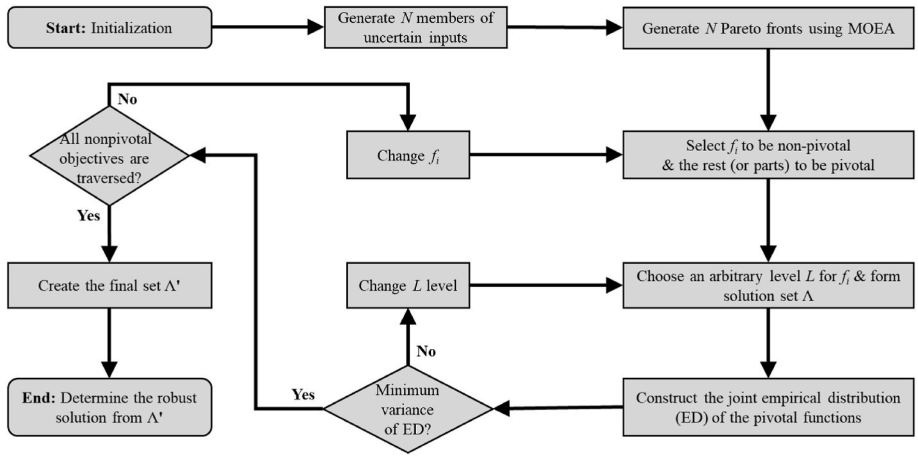

Fig. 4. Procedure of the robust multiobjective optimization and probabilistic analysis (ROPAR) algorithm for a general robust optimization problem.

problem formulation in achieving the objectives of the other formulations. By observing almost unchanged performance in the objective across various formulations, we gain insight into the stability of a specific robustness objective even when it is not considered in the formulation. Additionally, an analysis of the system's state behavior helps us understand why the same operating objectives respond differently to uncertain inflows under robust policies derived from different problem formulations.

For the second case, we benchmark against two other robustness optimization methods, previously applied by Quinn et al. (2017) and Watson and Kasprzyk (2017). Quinn et al. (2017)'s method is emblematic of Implicit Robust Optimization (IRO), which embeds the impact of uncertainty in a single Pareto front. Compared with IRO, ROPAR is associated with a higher computational burden because it performs full optimization for each sampled uncertainty realization but allows explicit propagation of uncertainty to the final solutions to be monitored. The method by Watson and Kasprzyk (2017), known as multi-scenario multi-objective robust decision making (Multi-scenario MORDM), shares similarities with ROPAR in treating each ensemble scenario independently. However, it differs in its approach to robustness metrics, favoring post-optimization analysis over ROPAR's direct optimization strategy. One of our aims is to demonstrate ROPAR's benefits over these traditional methods.

4. Results

4.1. Robust policies established with ROPAR

The Pareto front for each problem formulation is presented in the multidimensional objective space in Fig. 5. Each point signifies an optimal policy. Notably, the additional water diversion metric of interest, beyond the expected values, in both the *EV&SD*$_{WD}$ formulation (Fig. 5(c)) and the *EV&NRI*$_{WD}$ formulation (Fig. 5(d)), is manifested through color in the visual three-dimensional space.

In Fig. 5(a) - 5(d), a significant nonlinear tradeoff is observed between water diversion volume and hydrologic alteration degree. This tradeoff is quantifiable by the slope of the solution set in these two dimensions, where minor changes in hydrologic alteration markedly impact water diversion fluctuations. The tradeoff between alteration degree and hydropower generation is comparatively weak, and the tradeoff between water diversion and hydropower is the least significant. Crucially, substantial water diversion from this basin greatly disrupts the downstream water requirements, contrasting with the regulated water by reservoirs for hydropower, which is smoothly released downstream. In Fig. 5(b) - 5(d), the distribution of the upper solutions mirrors that in Fig. 5(a), but the bottom solutions are clustered in one block. Minor reservoir disturbances, such as an alteration degree near 0.25, lead to a more competitive generation-supply relationship.

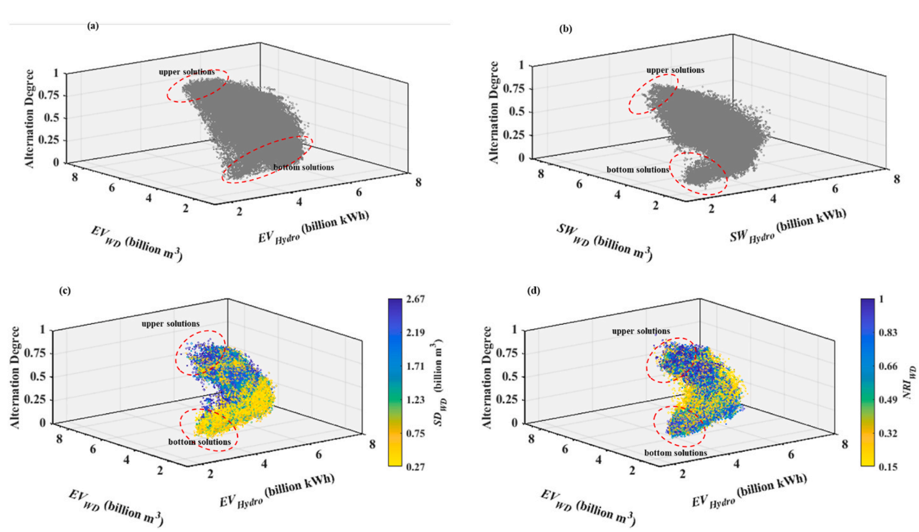

Fig. 5. Pareto frontier approximations for the formulations: (a) *EV*; (b) *SW*; (c) *EV&SD*$_{WD}$; (d) *EV&NRI*$_{WD}$. In Fig. 5(c) and (d), the performance of the fourth objective performance is represented by color. (For interpretation of the references to color in this figure legend, the reader is referred to the Web version of this article.)

Additionally, the magnitudes of the *SW* hydropower generation and water supply in Fig. 5(b) do not differ much from expected values, suggesting that the outcomes do not vary dramatically among years.

To further illustrate how the distribution of ROPAR solutions can serve as a preliminary indicator of solution robustness, we selected Fig. 5 (a) and (b) for detailed analysis, while Fig. 5(c) and (d) were omitted due to their similarity. In Fig. 5(a), the *EV* solutions cluster in the upper objective space and disperse in the lower space. This distribution indicates that policies with higher alteration are more effective in enhancing the adaptability of water diversion and hydropower generation to an uncertain external environment. The empirical distribution patterns of pivotal functions at two different levels of alteration (the nonpivotal function in our study), as illustrated in Fig. 6(a) and (c), further corroborate this insight. For a high alteration degree of 0.65, there is a 70% probability that the expected outcomes for hydropower and water diversion will fall within [5.32, 6.05] billion kWh and [6.08, 7.70] billion m^3, respectively, displaying a 'thin and tall' joint pdf. Less

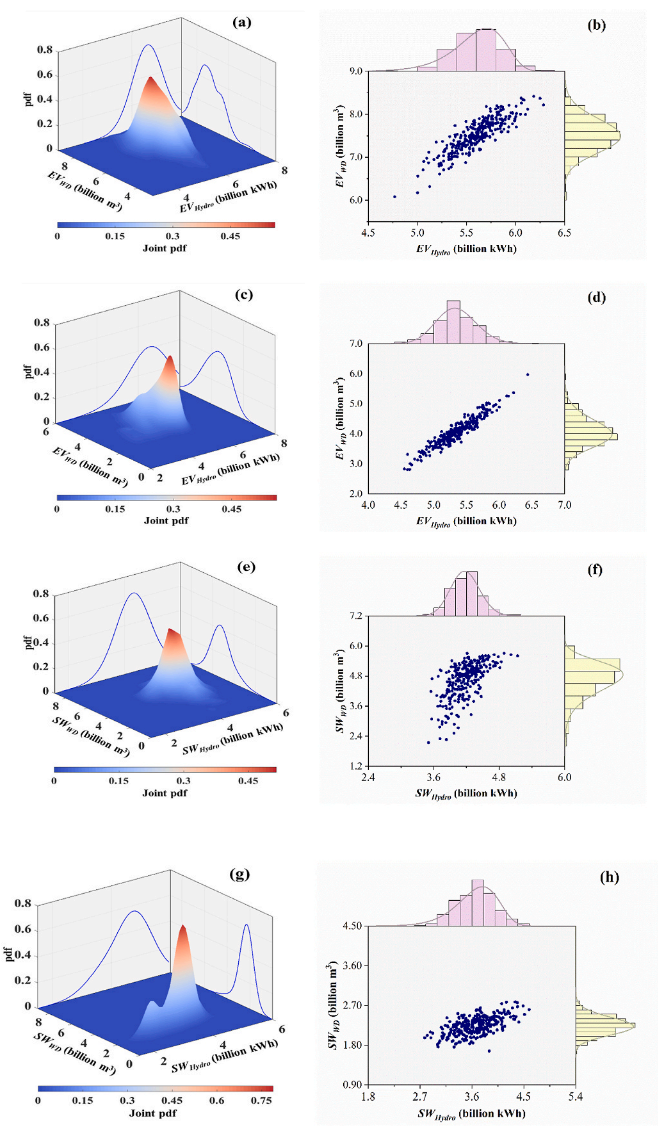

Fig. 6. Probability density functions (pdfs) of annual hydropower generation and water diversion. (a)–(d) are for the *EV* formulation, and (e)–(h) are for the *SW* formulation. (a) and (c), (e) and (g): joint empirical pdfs of solutions (based on a two-dimensional plane) for alteration degrees of 0.65 and 0.25, with marginal pdfs projected onto two coordinate axes; (b) and (d), (f) and (h): hydropower generation and water diversion distributions of randomly picked solutions over the synthetically optimized streamflow series.

variability is observed for hydropower compared to water diversion. With a lower alteration degree of 0.25, the 70% confidence intervals for hydropower and water diversion in Fig. 6(c) are [4.56, 5.67] billion kWh and [3.01, 4.50] billion m^3, respectively, with a 'short and fat' joint pdf. It results in an estimated annual economic loss of ~530 million RMB compared to the high-alteration alternative. However, the variability in water diversion is narrower in this formulation due to the generally lower water levels in the Danjiangkou Reservoir.

The joint pdfs of the pivotal hydropower and water diversion outcomes in *SW* at alteration degrees of 0.65 and 0.25 are depicted in Fig. 6 (e) and (g), respectively. The 70% confidence intervals for hydropower at these alteration levels are [3.91, 4.63] and [2.86, 4.10] billion kWh, and those for water diversion are [4.12, 5.84] and [1.80, 2.50] billion m^3, respectively. A single solution was randomly selected from each of Fig. 6(a), (c), 6(e), and 6(g) to represent the validation of the ROPAR probability. These were fed back into the synthetically optimized hydrological series, with the statistical results presented in Fig. 6(b), (d), 6 (f), and 6(h), respectively. The marginal distributions shapes closely align with those of the pdfs projected onto the coordinate axes in the left column of Fig. 6. Furthermore, we find that these scatter plots in Fig. 6 (d) and (h) exhibit good correlations in the absence of strong human interventions.

To identify robust solutions for each formulation, we select the level of 0.25 as the nonpivotal alteration degree in the *SW* formulation and 0.65 for other formulations to form the respective candidate set Λ', which corresponds to relatively narrow empirical pdfs of pivotal objectives across the synthetic hydrological ensemble (shown in Fig. 5(a)-5 (d)). The objective results for Λ' are then reported in Fig. 7a–d using parallel axes plots for clarity. These plots label an alternative solution as a shaded line that intersects each vertical axis at the value achievable across the synthetically optimized hydrological series. The axes are oriented such that the optimal direction is upward. All lines are shaded with respect to the hydropower objective performance, with darker shades indicating higher yields. The ideal solution for each set in Fig. 7 is therefore a dark horizontal line on the top of each axis. However, these lines commonly intersect between pairs of vertical axes, as superior performance for one objective comes at the cost of inferior performance for the other. Only a few solutions (dark lines) can achieve excellent power generation and moderate water supply at relatively mild degrees of alteration. The final robust optimal solution for each problem formulation is determined from these possible solutions, in reference to the local government's water management measures that aim to maximize the total economic benefit of pivotal hydropower and water supply (as detailed in section 3.1.1). The performance is summarized in Table 4, and it is observed that the robust $EV\&NRI_{WD}$ solution $p^*_\theta(EV\&NRI_{WD})$ we develop performs well, relative to other solutions across all considered objectives.

4.2. Verification of robust policies

The robust solutions from Table 4 were diagnosed using the out-of-sample streamflow set, with the results detailed in Table 5 and Fig. 8. Table 5 provides a 70% probability interval for the marginal distribution of the joint pdf across two different streamflow sets. The similarity in probability intervals between the optimization and out-of-sample sets indicates that the original probability analysis used in ROPAR was appropriate and reliable. In the *SW* formulation, hydropower variability exhibits some fluctuation; however, these are not substantial, particularly when compared to a worst-case formulation, where our tests revealed more severe deterioration in variability with larger sample sizes. The other water diversion metrics in the $EV\&SD_{WD}$ and $EV\&NRI_{WD}$ formulations exhibit reliable behavior, although they are not used as pivotal functions in determining robust solutions.

Fig. 8 provides the deterministic results for robust optimal policies across the hydrological ensemble series. This is drawn by evaluating

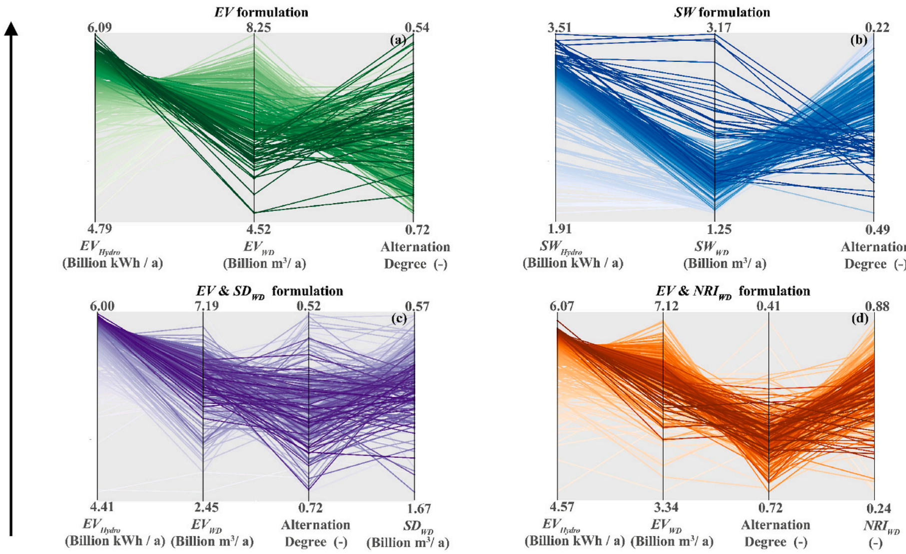

Fig. 7. Statistical results for all alternatives in the candidate set Λ': (a) *EV* formulation, (b) *SW* formulation, (c) $EV\&SD_{WD}$ formulation, and (d) $EV\&NRI_{WD}$ formulation.

Table 4
Simulation performance of the identified robust solutions for each of the four problem formulations with synthetically optimized streamflow series.

Solutions	Expected hydropower (billion kWh)	Expected water diversion (billion m^3)	Alteration degree (−)	Second-worst hydropower (billion kWh)	Second-worst water diversion (billion m^3)	SD_{WD} (billion m^3)	NRI_{WD} (−)
$p^*_\theta(EV)$	5.49	7.80	0.65	3.42	2.98	1.44	0.63
$p^*_\theta(SW)$	5.12	2.81	0.25	3.05	1.56	0.60	0.55
$p^*_\theta(EV\&SD_{WD})$	5.91	6.15	0.63	3.49	3.08	0.95	0.75
$p^*_\theta(EV\&NRI_{WD})$	5.74	6.45	0.62	3.46	3.71	0.81	0.84

Table 5
70% probability intervals for some objectives under the robust policies using both optimization and validation streamflow sets.

Solutions	Alteration degree	Objective	Optimization set			Validation set		
			Lower limit	Upper limit	Band width	Lower limit	Upper limit	Band width
$p^*_\theta(EV)$	0.65	J^{EV}_{Hydro} (billion kWh)	5.25	5.74	0.49	5.25	5.75	0.50
		J^{EV}_{WD} (billion m^3)	7.44	8.13	0.69	7.45	8.16	0.71
$p^*_\theta(SW)$	0.25	J^{SW}_{Hydro} (billion kWh)	3.31	3.91	0.60	3.30	3.94	0.64
		J^{SW}_{WD} (billion m^3)	1.72	2.12	0.40	1.74	2.14	0.40
$p^*_\theta(EV\&SD_{WD})$	0.63	$J^{EV\&SD_{WD}}_{Hydro}$ (billion kWh)	5.64	6.18	0.54	5.65	6.18	0.53
		$J^{EV\&SD_{WD}}_{WD}$ (billion m^3)	5.95	6.36	0.41	5.94	6.36	0.42
		$J^{EV\&SD_{WD}}_{SD_{WD}}$ (billion m^3)	0.73	1.16	0.43	0.73	1.16	0.43
$p^*_\theta(EV\&NRI_{WD})$	0.62	$J^{EV\&NRI_{WD}}_{Hydro}$ (billion kWh)	5.48	5.97	0.49	5.49	5.99	0.50
		$J^{EV\&NRI_{WD}}_{WD}$ (billion m^3)	6.27	6.64	0.37	6.26	6.65	0.39
		$J^{EV\&NRI_{WD}}_{NRI_{WD}}$ (−)	0.77	0.92	0.15	0.76	0.92	0.16

annual performance with the operator corresponding to each subplot. The first row shows the three *EV* objectives, while the second and third rows show the *SW* objectives and the additional water diversion metrics. To further validate the robustness framework's precision, robust control policies with expected alteration degrees of 0.35, 0.45, and 0.55 identified by ROPAR are examined. These policies are represented by points within the subplots that are positioned on the X-axis according to the objective values reached during the optimization set, and on the Y-axis according to the values reached in the out-of-sample validation set. Each subplot is oriented with the top-right corner denoting the optimal direction. Solutions that maintain consistent values during optimization and validation phases are aligned near the 1:1 line, marked by a black dashed line. A solution's performance is considered improved if it is located above this line during re-evaluation, and diminished if it falls below. Furthermore, Fig. 8 sheds light on the most suitable formulation for our case study. If the points derived from the proposed problem formulation consistently occupy the top-right regions across all subplots, specific attention to the formulation is warranted.

The deterministic results further confirm the consistency of the proposed framework, as evidenced by the clustering of most solutions near the 1:1 dashed line in Fig. 8, albeit with a few demonstrating improved or diminished performance upon re-evaluation. In Fig. 8(c), the points are concentrated around a few specific spots, illustrating that robust solutions reflect the overall long-term hydrological alteration degree well. Notably, annual average hydropower for these solutions, with alteration degrees ranging from 0.35 to 0.65, shows modest

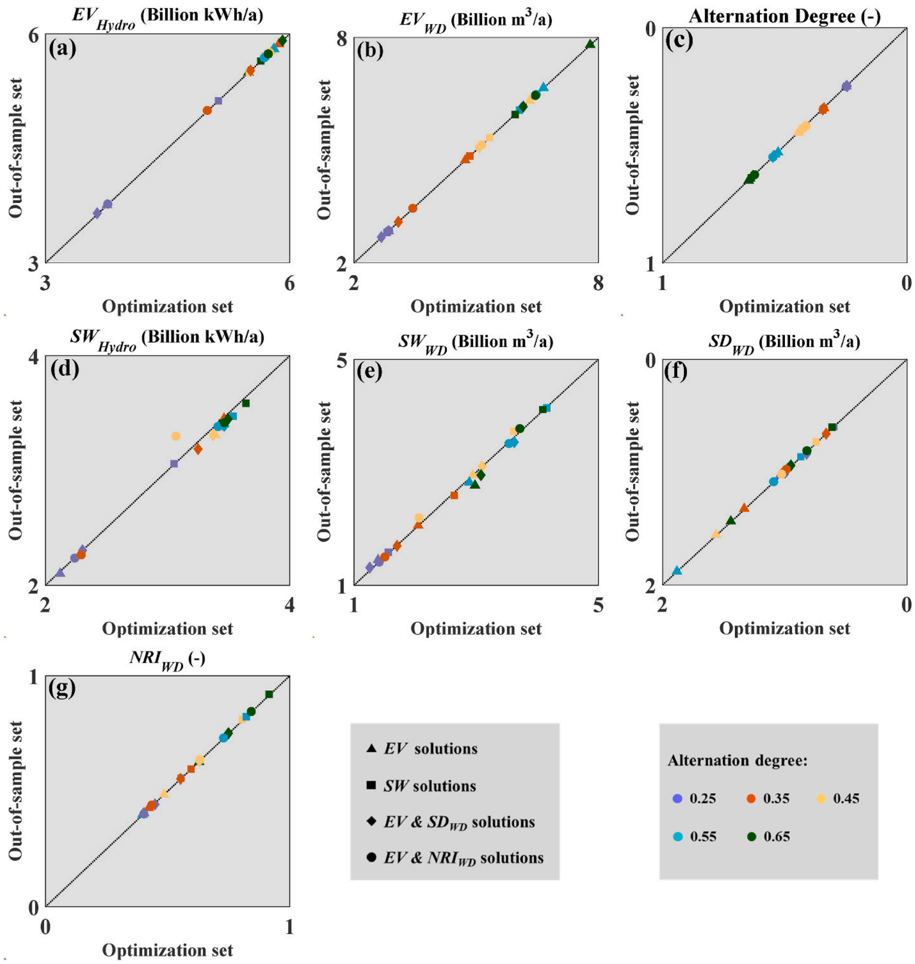

Fig. 8. Validation of robust solutions for each considered formulation (each subplot is oriented such that the optimal direction is toward the upper-right corner).

variation; this is evident from the clustering of points in the top-right corner of Fig. 8(a), suggesting a negligible impact on expected hydropower generation due to hydrological alterations. Conversely, the dispersion of points in Fig. 8(b) implies a greater influence of hydrological alterations on expected water diversion volumes. From an economic perspective, decision-makers favor high-alteration solutions, yet they must account for the adverse effects of these *EV* solutions on the standard deviation of water diversion, as shown in Fig. 8(f). Incorporating objectives related to interannual variability, such as the first-order moment of water diversion, allows high-alteration solutions to be more stable, albeit with some performance trade-offs with expected performance. The results align with Quinn et al. (2017), who demonstrated that water optimization problems factoring in the standard deviation of benefits in their objective functions yield more satisfactory policies. Moreover, the max-min criterion, a nonnegligible robustness metric in practical engineering (Maier et al., 2016), shows superior performance in the *SW* formulation compared to the $EV\&SD_{WD}$ formulation. This criterion, when combined with other robustness metrics through our proposed *NRI*, can enhance outcomes. As observed in Fig. 8 (g), the optimal *NRI* reaches 0.84, corresponding to an *SW* annual water diversion of 3.71 billion m^3 and a standard deviation of 0.81 billion m^3. These represent improvements of 24.5% and 43.7%, respectively, over the *EV* formulation, but incur an additional cost of approximately 123 million RMB.

The final component of the first verification module involves evaluating the time-varying probabilistic behavior of the reservoir system under these robust ROPAR policies. Fig. 9 presents the likelihood of various reservoir water levels across the validation flow set in logarithmic space. The colors red, yellow, and blue correspond to high, moderate, and low probabilities, respectively. Across all solutions, water levels are maintained below flood control limits and within permissible operating ranges. However, the overall shapes of these time-varying pdfs show significant differences. Tracing the highest probability streak in red, Fig. 9(c) and (d) reveal that under the robust *SW* policy, Ankang Reservoir water level remains consistently high throughout the year. This elevation aids power generation and diminishes downstream flow to the Danjiangkou Reservoir, particularly after the monsoon season, leading to lower water levels in Danjiangkou with restricted diversion. In Fig. 9(a)-9(b), the robust *EV* policy, targeting high flow alteration, will improve water diversion volume primarily by raising Danjiangkou Reservoir water level during the nonflood season, which inevitably lowers the water level at Ankang Reservoir. Affected by intensive human interventions, interannual water level variations in both reservoirs exhibit high uncertainty, with yellow and red colors (moderate to high probability) over the entire feasible interval. The compromise $EV\&NRI_{WD}$ formulation demonstrates more balanced behavior than the first two strategies. The Ankang Reservoir water level in the red high-probability region (Fig. 9(e)) remains high from May to September due to monsoonal rainfall. With the significant decrease in precipitation at the end of the rainy season, the Ankang Reservoir water level begins to drop but remains moderate during the dry season. It ensures that the Danjiangkou Reservoir water level is in the upper middle zone in Fig. 9 (f) for sufficient water diversion via the MSWT project.

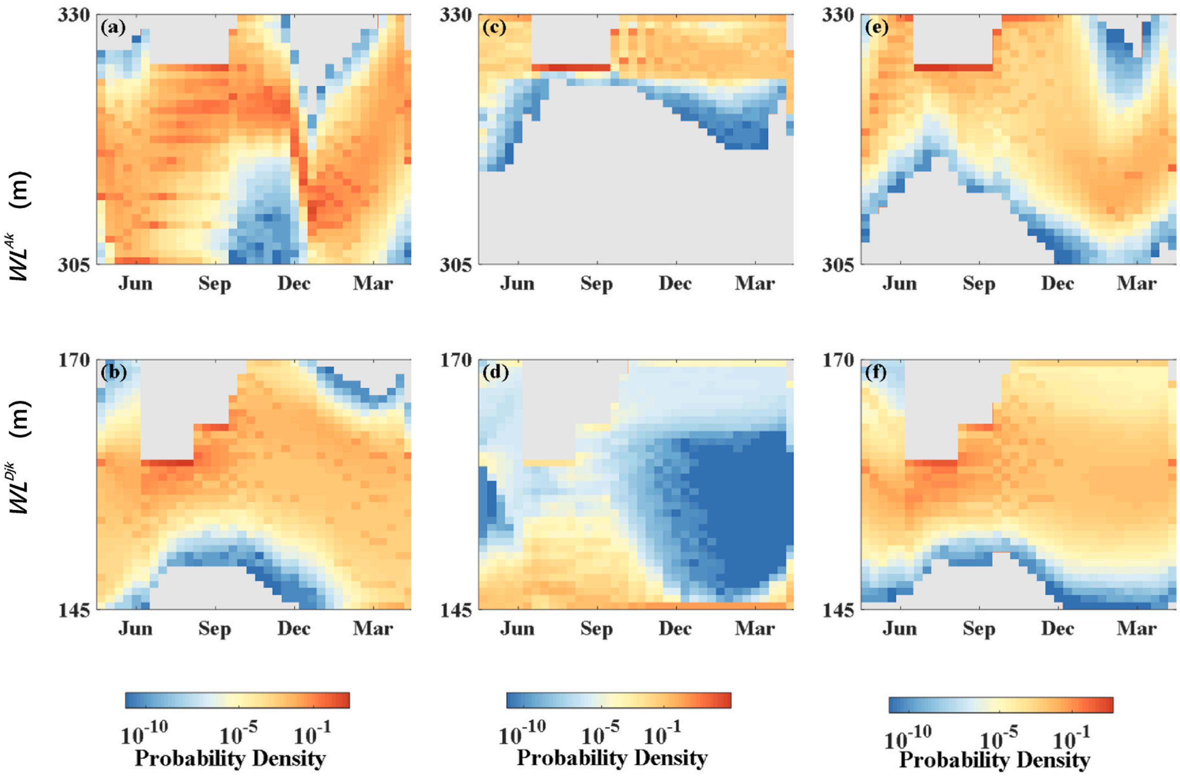

Fig. 9. Probabilistic trajectories of the water levels in the cascade reservoir system for three selected robust solutions from the *EV* (a–b), *SW* (c–d) and $EV\&NRI_{WD}$ (e–f) formulations.

4.3. Comparison with other representative optimization methods

In this section, an in-depth analysis of ROPAR against other representative optimization methods is given in terms of the computational cost and optimization results. Given that all optimization methods require model runs, the computational cost of these methods is expressed by the total number of function evaluations (*NFE*), assuming the same cost for a single function evaluation.

The *NFE* of ROPAR primarily entails the generation of Pareto fronts (Step 1 in section 3.3) and the determination of the robust solution (Steps 2–7). As the stopping criterion for obtaining one Pareto front set in our study is to reach a prespecified number (*ne*) of evaluations of the objective functions, the *NFE* for full Pareto optimization is derived as N^*ne, where N is the number of samples with the uncertain input. To find the robust solution from the set of N solutions at level L, the number of remaining model runs is N^*N. If analyses are performed for several (*nl*) levels of nonpivotal functions, the remaining *NFE* is nl^*N^2. Consequently, the total *NFE* of all ROPAR steps is $N^*ne + nl^*N^2$. The IRO method (Quinn et al., 2017) uses a mean operator to filter each synthetic ensemble in a round of optimization, requiring only *ne* evaluations of the objective function. However, each evaluation of the objective function requires N executions of the complex operating model (equal to the number of input samples). As such, the *NFE* of IRO is N^*ne. Note that the value of *ne* is usually set large enough for the algorithm to converge, and the additional term nl^*N^2 in ROPAR can be disregarded if $ne \gg nl^*N$. Multi-scenario MORDM performs the same full Pareto optimization procedure as ROPAR. The *NFE* of this part is N^*ne if the number of its reference scenarios is the same as ROPAR for a fair comparison (Watson and Kasprzyk, 2017). In its subsequent post-optimization analysis, each candidate solution for each scenario is fed into the *N*-scenario ensemble for robustness evaluation. The *NFE* of this part is pop^*N^2, where *pop* is the population size of NSGA-III. The total *NFE* of Multi-scenario MORDM is therefore $N^*ne + pop^*N^2$. All these *NFE*s are close, and the efficiency of all methods can be improved with parallelized versions. In the ensemble member loop of a parallel ROPAR, each deterministic NSGA-III can be run independently by using a cluster of several computers or cloud computing services.

Regarding the optimization outcomes, the IRO solutions lack a clear visual representation that could elucidate which Pareto direction offers greater robustness (detailed in Text S4). In the $EV\&NRI_{WD}$ problem formulation, we select a solution from the IRO's single Pareto front that is closest to a hydrological degree of 0.62. This level matches the

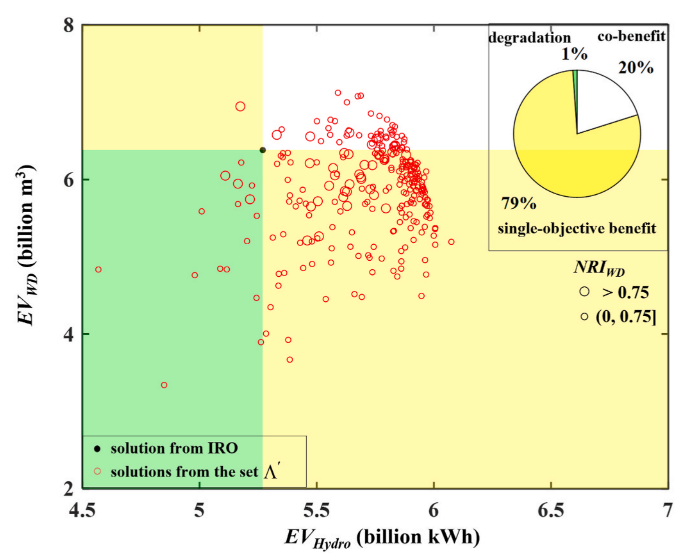

Fig. 10. Hydropower generation, water diversion and *NRI* performance achieved through the optimal IRO solution (black circle) and the robust candidate set Λ' (red circles) identified in the $EV\&NRI_{WD}$ formulation by ROPAR. (For interpretation of the references to color in this figure legend, the reader is referred to the Web version of this article.)

hydrological degree of the ROPAR solution $p_\theta^*(EV\&NRI_{WD})$, thereby serving as a fair comparison of methods. Fig. 10 illustrates the performance results for hydropower, water diversion and *NRI* estimates of the IRO solution (black circle) and robust candidate set Λ' (red circles) identified in $EV\&NRI_{WD}$ by ROPAR. Depending on each synthetic member of the validation set, the ROPAR solutions in Λ' might produce co-benefits or degrade performance compared to the IRO solution. Of the results, 20% of the 300 alternatives in the white region show improved performance for all operating objectives. For the remaining solutions, performance typically improves for one objective but deteriorates for the others (e.g., the yellow region accounting for 79% of the robust candidates). Similar findings are observed in the other three problem formulations as well (refer to Text S5), further substantiating ROPAR's superiority over IRO with comparable *NFE*s.

When employing the three operating objectives from the *EV* formulation alongside the *NRI* as a robustness metric, the Pareto fronts in the first *EV* problem formulation in section 4.1 can offer alternative candidates for Multi-scenario MORDM. Following the approach of Watson and Kasprzyk (2017), we re-evaluated all alternatives in Fig. 5(a) focusing solely on the *NRI* robustness metric. The solution yielding the highest *NRI* is identified as the final policy for Multi-scenario MORDM. This policy exhibits a hydrological alteration degree of 0.53, showing a bias compared to the ROPAR solution $p_\theta^*(EV\&NRI_{WD})$, and reveals a broader joint pdf for hydropower and water diversion, with 70% confidence intervals of [4.91, 5.53] billion kWh and [5.05, 5.66] billion m^3, respectively. The optimal *NRI* stands at 0.78, corresponding to the second worst, and the standard deviation of water diversion being 3.37 and 0.85 billion m^3, respectively. All water diversion performances and expected hydropower generation of Multi-scenario MORDM fall short of those in $p_\theta^*(EV\&NRI_{WD})$. This comparative underperformance of Multi-scenario MORDM against ROPAR underscores the importance of developing our *NRI*-based robustness formulation.

5. Discussion and conclusions

The substantial uncertainty associated with the future state of the world will make the long-term planning and management of water resource systems challenging. To address this issue, advanced robust optimization techniques are critical in identifying policies that are insensitive to variations in exogenous disturbances. In this context, we utilize and improve the EMODPS method, which not only facilitates an explicit visualization of model uncertainty propagation with the ROPAR algorithm developed by Marquez and Solomatine (2019), but also enables the generalization of policies through the integration of an additional out-of-sample verification module. Furthermore, we develop four different robustness problem formulations to explore the implications of various stakeholder objectives. With a specific case illustration of the cascade reservoirs in the Hanjiang River basin in China, some important conclusions are drawn.

(1) The ROPAR algorithm combined with EMODPS performs a full multiobjective optimization method to explicitly describe how uncertainty is propagated to the Pareto-optimal solutions and allows for subsequent probabilistic analyses. It is possible to intuitively identify solution sets with different levels of robustness to input uncertainty and to select robust solutions according to the preferences of decision-makers. In our four robustness formulations with hydrological alteration degree serving as the nonpivotal function, we find that two different extremes (approximately 0.65 and 0.25, respectively) are preferred for minimizing uncertainty in pivotal functions (i.e., hydropower and water diversion).

(2) Through an additional verification module with an out-of-sample streamflow set, the optimal ROPAR policies have been validated robust. However, different quantitative formulations of operating objectives in the reservoir system may yield different results in policy extraction. Among the four problem formulations, our developed *NRI*-based formulation (i.e., $EV\&NRI_{WD}$) can successfully integrate various robustness metrics, thereby achieving an effective balance among all considered objectives.

(3) Taking two common optimization methods (i.e., IRO and Multi-scenario MORDM) as benchmarks, we perform a systematic analysis of them and ROPAR in terms of both computational costs and optimization results. The comparison shows that ROPAR outperforms them in finding more robust solutions, and the computational cost in its design can be reduced by processing each member of the considered ensembles in parallel.

In summary, these findings provide critical insights into how ROPAR within the EMODPS framework can facilitate explicit tradeoffs among multiobjective cascade reservoir operations. Yet, due to limitations in the length of the paper, several intriguing results were not fully explored. For instance, in our *EV* formulation, with increasing water diversion volumes, the variability of hydropower generation was unexpectedly narrower compared to water diversion. This could be attributed to frequent fluctuations in the Danjiangkou Reservoir's water level across different division zones (as shown in Figs. 1 and 9(b)), which affect the quantities of diverted and discharged water, while hydropower generation is only constrained by maximum and minimum output limits. Future research could focus on deconstructing the robust operating policy to analyze the sensitivity of different objectives to each input variable (Quinn et al., 2019). Additionally, the robustness of our ROPAR policies requires reevaluation in broader sampled scenarios for nonstationary inflow changes, even considering more deeply uncertain factors associated with cascade reservoir systems (Bertoni et al., 2019). To address this, more plausible future scenario generators, such as those incorporating variability in streamflow generator parameters, should be integrated within our explicit optimization framework. Finally, developing more prescriptive formulations of robustness metrics for operating objectives can further improve the effectiveness of robust optimization endeavors and acceptance of results by decision-makers.

CRediT authorship contribution statement

Shaokun He: Writing – original draft, Visualization, Validation, Software, Resources, Project administration, Methodology, Investigation, Funding acquisition, Formal analysis, Data curation, Conceptualization. **YiBo Wang:** Software, Investigation, Formal analysis, Data curation. **Dimitri Solomatine:** Writing – review & editing, Supervision, Methodology. **Xiao Li:** Writing – review & editing, Visualization, Validation, Supervision, Resources, Methodology, Data curation.

Software and data availability

Raw streamflow data can be accessed from the Hydrological Bureau of the Yangtze Water Resources Commission of China (http://www.cjh.com.cn). The open-source Kirsch-Nowak Streamflow Generator code using python language (version 3.10) can be founded in Github: https://github.com/julianneq/Kirsch-Nowak_Streamflow_Generator. Our ROPAR algorithm code using the Matlab language can be found in the website: https://zenodo.org/records/13932517. Author's experimental environment was as follows.

— OS: Windows 11
— CPU: Intel(R) Core (TM) i7-9700 3.00 GHz
— RAM: 64.00 GB
— GPU: NVIDIA GeForce RTX 3090

Data Availability Statement

See link in "Software and data availability".

Declaration of competing interest

The authors declare that they have no known competing financial interests or personal relationships that could have appeared to influence the work reported in this paper.

Acknowledgments

The study is financially supported by National Key R&D Program of China (2023YFC3206005, 2023YFC3209502), National Natural Science Foundation of China (grant no. 52269003, U2340217), and the China Postdoctoral Science Foundation (2022M711493). Part of this study was conducted during the first author's internship at IHE Delft Institute for Water Education in the Netherlands, funded by the China Scholarship Council (201906270112).

Appendix A. Supplementary data

Supplementary data to this article can be found online at https://doi.org/10.1016/j.envsoft.2024.106301.

References

Bertoni, F., Castelletti, A., Giuliani, M., Reed, P.M., 2019. Discovering Dependencies, trade-offs, and robustness in joint dam design and operation: an ex-post assessment of the kariba dam. Earth's Future 7 (12), 1367–1390.
Bonham, N., Kasprzyk, J., Zagona, E., Smith, R., 2024. Interactive and multimetric robustness tradeoffs in the Colorado River Basin. J. Water Resour. Plann. Manag. 150 (3), 05023025.
Dariane, A.B., Ghasemi, M., Karami, F., Azaranfar, A., Hatami, S., 2021. Crop pattern optimization in a multi-reservoir system by combining many-objective and social choice methods. Agric. Water Manag. 257, 107162.
Deb, K., Gupta, H., 2006. Introducing robustness in multi-objective optimization. Evol. Comput. 14 (4), 463–494.
Deb, K., Jain, H., 2014. An evolutionary many-objective optimization algorithm using reference-point-based nondominated sorting approach, part I: solving problems with box constraints. IEEE Trans. Evol. Comput. 18 (4), 577–601.
Giuliani, M., Castelletti, A., 2016. Is robustness really robust? How different definitions of robustness impact decision-making under climate change. Climatic Change 135 (3–4), 409–424.
Giuliani, M., Castelletti, A., Pianosi, F., Mason, E., Reed, P.M., 2016. Curses, tradeoffs, and scalable management: advancing evolutionary multiobjective direct policy search to improve water reservoir operations. J. Water Resour. Plann. Manag. 142 (2), 04015050.
Giuliani, M., Quinn, J.D., Herman, J.D., Castelletti, A., Reed, P.M., 2018. Scalable multiobjective control for large-scale water resources systems under uncertainty. IEEE Trans. Control Syst. Technol. 26 (4), 1492–1499.
He, S., Chen, K., Liu, Z., Deng, L., 2023. Exploring the impacts of climate change and human activities on future runoff variations at the seasonal scale. J. Hydrol. 619, 129382.
He, S., Guo, S., Yin, J., Liao, Z., Li, H., Liu, Z., 2022a. A novel impoundment framework for a mega reservoir system in the upper Yangtze River basin. Appl. Energy 305, 117792.
He, S., Guo, S., Zhang, J., Liu, Z., Cui, Z., Zhang, Y., Zheng, Y., 2022b. Multi-objective operation of cascade reservoirs based on short-term ensemble streamflow prediction. J. Hydrol. 610, 127936.
Jaiswal, R.K., Lohani, A.K., Tiwari, H.L., 2021. A decision support system framework for strategic water resources planning and management under projected climate scenarios for a reservoir complex. J. Hydrol. 603, 127051.
Kapelan, Z.S., Savic, D.A., Walters, G.A., 2005. Multiobjective design of water distribution systems under uncertainty. Water Resour. Res. 41 (11), W11407.
Kirsch, B.R., Characklis, G.W., Zeff, H.B., 2013. Evaluating the impact of alternative hydro-climate scenarios on transfer agreements: practical improvement for generating synthetic streamflows. J. Water Resour. Plann. Manag. 139 (4), 396–406.
Kwakkel, J.H., Eker, S., Pruyt, E., 2016. How robust is a robust policy? Comparing alternative robustness metrics for robust decision-making, robustness analysis in decision aiding. Optimization, and Analytics. Springer International Publishing, Cham, pp. 221–237.
Labadie, J.W., 2004. Optimal operation of multireservoir systems: state-of-the-art review. J. Water Resour. Plann. Manag. 130 (2), 93–111.
Laplace, P.S., Simon, P., 1951. A philosophical essay on probabilities. Translated from the 6th French Edition by FrederickWilson Truscott and Frederick Lincoln Emory.
Long, D., Yang, W., Scanlon, B.R., Zhao, J., Liu, D., Burek, P., Pan, Y., You, L., Wada, Y., 2020. South-to-North Water Diversion stabilizing Beijing's groundwater levels. Nat. Commun. 11 (1), 3665.
Maier, H.R., Guillaume, J.H.A., van Delden, H., Riddell, G.A., Haasnoot, M., Kwakkel, J. H., 2016. An uncertain future, deep uncertainty, scenarios, robustness and adaptation: how do they fit together? Environ. Model. Software 81, 154–164.
Marquez Calvo, O.O., 2020. Advancing Robust Multi-Objective Optimisation Applied to Complex Model-Based Water-Related Problems. Taylor & Francis Group, Milton, UNITED KINGDOM.
Marquez, O.O., Solomatine, D.P., 2019. Approach to robust multi-objective optimization and probabilistic analysis: the ROPAR algorithm. J. Hydroinf. 21 (3), 427–440.
McPhail, C., Maier, H.R., Kwakkel, J.H., Giuliani, M., Castelletti, A., Westra, S., 2018. Robustness metrics: how are they calculated, when should they be used and why do they give different results? Earth's Future 6 (2), 169–191.
McPhail, C., Maier, H.R., Westra, S., van der Linden, L., Kwakkel, J.H., 2021. Guidance framework and software for understanding and achieving system robustness. Environ. Model. Software 142, 105059.
Mohanty, M., Tare, V., 2022. Anthropogenic interventions in watersheds on river flow health: assessment using Bootstrapped Principal Component analysis. J. Water Resour. Plann. Manag. 148 (1), 04021094.
MWR, 2016. The designed operation rules of Danjiangkou reservoir for water diversion. Water Resources and Hydropower Press. Beijing (in Chinese).
Nowak, K., Prairie, J., Rajagopalan, B., Lall, U., 2010. A nonparametric stochastic approach for multisite disaggregation of annual to daily streamflow. Water Resour. Res. 46 (8), W08529.
Pinto, J.W.O., Afonso, S.M.B., Willmersdorf, R.B., 2019. Robust optimization formulations for waterflooding management under geological uncertainties. J. Braz. Soc. Mech. Sci. Eng. 41 (11), 475.
Quinn, J.D., Reed, P.M., Giuliani, M., Castelletti, A., 2017. Rival framings: a framework for discovering how problem formulation uncertainties shape risk management trade-offs in water resources systems. Water Resour. Res. 53 (8), 7208–7233.
Quinn, J.D., Reed, P.M., Giuliani, M., Castelletti, A., 2019. What is controlling our control rules? Opening the black box of multireservoir operating policies using time-varying sensitivity analysis. Water Resour. Res. 55 (7), 5962–5984.
Roach, T., Kapelan, Z., Ledbetter, R., Ledbetter, M., 2016. Comparison of robust optimization and Info-Gap methods for water resource management under deep uncertainty. J. Water Resour. Plann. Manag. 142 (9), 04016028.
Savage, L.J., 1951. The theory of statistical decision. J. Am. Stat. Assoc. 46 (253), 55–67.
Sunkara, S.V., Singh, R., Gold, D., Reed, P., Bhave, A., 2023. How should diverse stakeholder interests shape evaluations of complex water resources systems robustness when confronting deeply uncertain changes? Earth's Future 11 (8), e2022EF003469.
Wang, L., Xu, B., Zhang, C., Chen, X., Zheng, Y., Zhang, J., Fu, G., 2023. Exploring the trade-offs among hydropower benefits, environmental flow, and surface water temperature in a large reservoir under deep uncertainty. J. Hydrol. 624, 129913.
Watson, A.A., Kasprzyk, J.R., 2017. Incorporating deeply uncertain factors into the many objective search process. Environ. Model. Software 89, 159–171.
Wu, W., Eamen, L., Dandy, G., Razavi, S., Kuczera, G., Maier, H.R., 2023. Beyond engineering: a review of reservoir management through the lens of wickedness, competing objectives and uncertainty. Environ. Model. Software 167, 105777.
Yu, X., Xu, Y.-P., Gu, H., Guo, Y., 2023. Multi-objective robust optimization of reservoir operation for real-time flood control under forecasting uncertainty. J. Hydrol. 620, 129421.
Zhang, G., Gu, H., Wang, W., Zhang, S., Xue, L., 2024a. Evaluation of subdaily hydrological regime alteration characteristics for hydro–photovoltaic complementary operation in the upper yellow river. Water 16 (2), 300.
Zhang, J., Solomatine, D., Dong, Z., 2024b. Robust multi-objective optimization under multiple uncertainties using the CM-ROPAR approach: case study of water resources allocation in the Huaihe River basin. Hydrol. Earth Syst. Sci. 28 (16), 3739–3753.